Stress Intensity Factor of Wood from Crack-Tip Displacement Fields Obtained from Digital Image Processing

Sandhya Samarasinghe and Don Kulasiri

Stress intensity factor of radiata pine (*Pinus radiata*) in Tangential-Longitudinal opening mode was determined from crack-tip displacement fields obtained from digital image correlation in conjunction with orthotropic fracture theory. For lower loads, experiments agreed with the linear elastic fracture theory but for higher loads, stress intensity factor and load relationship was nonlinear. For 41% of the specimens tested, tip-displacement based stress intensity factor agreed with that based on the ASTM standard formula for lower loads but deviated for higher loads closer to failure. The tip displacement plots showed that the nonlinear behaviour is due to large displacements which we attributed to large plastic deformations and/or micro-cracking in this region. The other 59% specimens showed a similar trend except that the crack-tip based stress intensity factor was consistently higher than the value obtained from the standard formula. The fracture toughness from tip displacements was larger than the standard values for all specimens and the two were related by a logarithmic function with an R^2 of 0.61. The study also established that fracture toughness increases with the angle of inclination of the original crack plane to the Radial Longitudinal plane.

1 Introduction

Structural wood members contain natural or artificial defects such as knots, drying checks, splits, and machined notches and holes that become stress raisers within the material. The strength of cracked bodies is represented by the critical stress intensity factor (fracture toughness) which is a material property. In the study of fracture, three fracture modes are generally specified: opening (Mode I), shearing (Mode II), and twisting (Mode III). In opening mode forces are applied perpendicular to crack and in the other two modes shearing and twisting forces, respectively, are applied at the tip. Each of these modes is characterized by a stress intensity factor,

K_I, K_{II}, and K_{III}, respectively, which indicates the level of stress increase in the vicinity of a crack. For an orthotropic material like timber, there are six fracture systems for the three orthotropic planes but in many practical situations, fracture is relevant in Tangential-Longitudinal (TL) and Radial Longitudinal (RL) planes only and many a time fracture occurs in mixed-mode. (Here, first letter denotes direction normal to crack plane and second denotes direction of crack.) In this paper, a detailed study of mode-I fracture in TL system is reported. Here, the force is applied in Tangential (T) direction, crack width is in Radial (R) direction and crack propagates in Longitudinal (L) direction in RL plane.

The early investigators (Griffith, 1920, Westergaard, 1948, Irwin 1957, 1961) laid the foundation for the mathematical analysis of fracture and crack tip stress and displacements in isotropic materials. Later Sih et al. (1965) developed a fracture theory for orthotropic materials and developed mathematical formulae for crack tip stress and displacement fields in these materials. These formulae could provide a more accurate estimate of stress intensity factor than that based on the ASTM standard formulae if the crack tip displacements can be measured accurately. The digital image correlation has been established as a useful tool for measuring surface displacement fields in materials. In our earlier work, we presented the displacement fields in wood in parallel- and perpendicular-to-grain tension using digital image correlation. (Samarasinghe and Kulasiri 2000a). In it we reported that lignin behaves like rubber in tension and that tracheids show complex behaviour. We also reported and compared theoretical and experimental crack-tip displacement fields in wood with a crack either parallel- or perpendicular-to-grain (Samarasinghe and Kulasiri 2000b). There we showed that linear elastic orthotropic fracture theory captures the overall trend of the experimentally observed displacement pattern but the experimental pattern showed more complex variations within the overall pattern and we attributed them, with reasoning, to cellular interactions that is not captured by the theory.

The goal of the work described in this paper is to extend these studies further by using digital image correlation to obtain full field displacement fields near a crack tip in wood subject to tension

and use them in conjunction with the linear elastic orthotropic fracture theory and representative material properties to obtain stress intensity factors for wood (K_{ITL}). The experimental stress intensity factor is compared to that obtained from the ASTM standard (1995) formula involving a finite geometry correction factor. The advantage of the proposed method is that the stress intensity factor thus derived does not need to be corrected for the finite geometry of the member the crack is in. The proposed method is a scientific investigation to determine stress intensity factor from local crack tip deformation and not a method for industrial grading of lumber.

In most practical situations truly orthotropic conditions are not realized and therefore, the geometric axes of a member may not coincide with the axes of material symmetry. Thus, in a practical TL crack system original crack plane may not lie in the RL plane. Our earlier work (Samarasinghe and Kulasiri 2000a, b and Mall et al. 1983) stated that a crack in this situation will *eventually* propagate along the RL plane, which is the weakest material plane, and this inclination of the original crack plane to the RL plane could affect the stress intensity factor. For example, if a crack lies in the RL plane, stress intensity factor is smaller than that for a crack inclined to the RL plane. In this paper, we establish the fact that this angle has a strong influence on the critical stress intensity factor.

2 Objectives

The objectives of the research described here are to:

1) Determine stress intensity factors for wood subject to tension in a practical TL Mode-I crack system using displacement fields obtained from digital image correlation in conjunction with theoretical orthotropic fracture formulae and representative material properties,

2) Compare experimental stress intensity factor with that obtained from the ASTM standard formula, and

3) Study the effect of the angle of inclination of the original crack plane to the RL plane on the critical stress intensity factor.

3 Background and Methodology

3.1 Theoretical Stress Intensity Factor Formulae for Orthotropic Materials

In 1965, Sih et. al. formulated stress and displacement fields near the tip of a remotely loaded orthotropic plate in tension (Fig. 1). This derivation assumes that the material is homogeneous, truly orthotropic, and obeys linear elastic fracture theory that is valid only if crack tip plastic region is relatively small. The theory also assumes that the crack lies in a plane of material symmetry and that the direction of crack propagation coincides with this plane. The crack opening mode displacement for an orthotropic plate remotely loaded in tension is given by (Sih et al. 1965) as:

$$v = \tag{1}$$

$$K_I \sqrt{2\pi r}\, \mathrm{Re}\left[\frac{1}{\mu_1 - \mu_2}(\mu_1 q_2 \sqrt{Cos\theta + \mu_2 Sin\theta} - \mu_2 q_1 \sqrt{Cos\theta + \mu_1 Sin\theta}) \right]$$

where v is vertical displacement, in the direction perpendicular to the crack, of a point lying a distance r and angle θ from the tip (Fig. 1), K_I is mode-I stress intensity factor, Re is the real value of the expression within square brackets, and μ_1, μ_2, q_1, q_2 are functions of material properties. The values of μ_1, μ_2, q_1 and q_2 are the complex roots of the characteristic equation (Eq. 2), as specified in detail in Sih et al. 1965, which corresponds to the governing differential equation for a remotely applied load with the boundary conditions specified as in Fig. 1.

$$b_{11}\mu^4 + (2b_{12} + b_{66})\mu^2 + b_{22} = 0 \tag{2}$$

where for TL mode of loading for wood,

$$b_{11} = \frac{1}{E_L} - \frac{v_{RL}{}^2}{E_R}; \quad b_{22} = \frac{1}{E_T} - \frac{v_{RT}{}^2}{E_R}$$

$$b_{12} = -\left[\frac{v_{TL}}{E_T} + \frac{v_{RL}v_{RT}}{E_R} \right]; \quad b_{66} = \frac{1}{G_{LT}}$$

The parameter E with subscripts denotes Young's modulus in L, R, T directions, v with subscripts denotes poisson ratio in TL, RL, and RT planes, and G_{LT} is the shear modulus in LT plane. Appen-
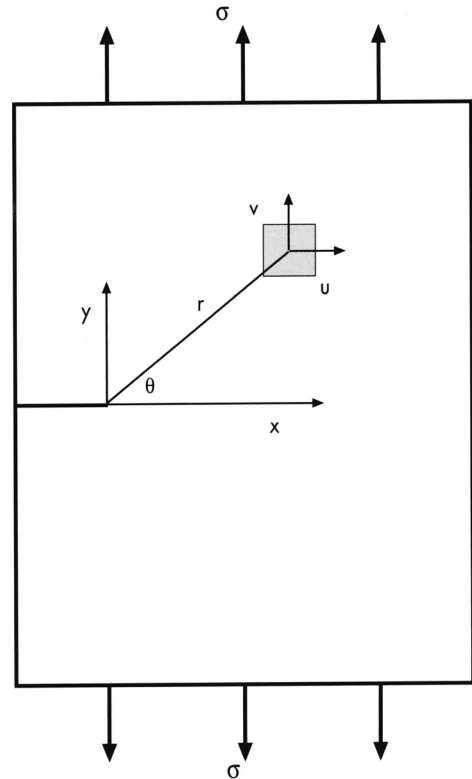

Fig. 1. Two dimensional near tip displacement components of a unit area in a plate loaded in tension.

dix I provides a list of definitions of the terms in these formulae.

Eq. 1 shows that the theoretical displacement at a point near the crack tip of a truly orthotropic material obeying linear elastic fracture theory is uniquely defined by a constant stress intensity factor. Before applying the theoretical formulae to wood, the implications of the assumptions in the derivation need to be addressed. Firstly, the theory assumes uniform material properties. Triboulot et al. (1984) showed that for constant average orthotropic wood properties, near tip stresses obtained from the finite element method and the analytical formulae are similar. However, it is well known from wood literature that wood properties vary significantly from early wood to latewood, from pith to the bark, and along the height of the stem (Bodig and Jayne 1982). Secondly, the theory assumes true orthotropy. However, wood is not truly orthotropic unless the member is cut farther

away from the center of a large diameter stem and therefore, as stated earlier, an induced crack may not always lie in a plane of material symmetry.

Finally, with regard to the applicability of the linear elastic fracture theory to wood, it has been generally accepted that the theory applies and the standard formulae have been used to obtain fracture toughness values for wood. The standard formula is valid only if the region of plastic deformation near the crack-tip is relatively small compared to the elastic stress field. However, no studies have been conducted to investigate the existence or the size of the crack tip plastic region in wood.

3.2 Standard Stress Intensity Factor Formulae

The standard stress intensity factor formulae relate the stress intensity factor to the crack geometry and the remotely applied stress, and are widely used to obtain fracture toughness for materials including wood. The origin of the standard stress intensity factor formula for a crack in a remotely loaded orthotropic plate has been the same governing equations applied to formulate crack-tip displacements in Eq. 1. The standard formula applies for conditions of much larger overall width and thickness compared to the crack length. However, all structural members have finite geometry and to account for the width effect, a geometry correction factor has been incorporated into the formula. For an edge notched tensile specimen the ASTM (1995) standard relationship is given as

$$K_I = F \, \sigma \sqrt{\pi a} \tag{3}$$

where, a is crack length, σ is applied remote stress, and F is the geometry correction factor which is a function of the ratio of crack length, a, to the width of the specimen, w. A formula for F is given in stress intensity factor handbooks (Tada et al. 1985) as:

$$F = 1.12 - 0.231 \left(\frac{a}{w} \right) + 10.55 \left(\frac{a}{w} \right)^2 - 21.72 \left(\frac{a}{w} \right)^3 + 30.95 \left(\frac{a}{w} \right)^4 \tag{4}$$

As for correction factors, formulae such as Eq. 4 developed for isotropic materials are commonly used for wood. These have been derived from either finite element method or boundary collocation methods. However, Mall et al. (1983) have pointed out that these factors for wood can be affected by the directional wood properties. However, if the stress intensity factor is obtained from Eq. 1 in conjunction with the measured crack tip displacements, no correction is needed since a very small region near the crack tip is considered and therefore, more reliable estimates of the stress intensity factor can be expected. The stress intensity factor thus derived may be compared with that obtained from the standard formula (Eq. 3) and issues related to the use of the two approaches can be addressed.

3.3 Digital Image Correlation

Digital Image Correlation (DIC) is a non-contacting measuring technique that has been developed to obtain full field surface displacements and their gradients (strains) of objects under stress. The DIC method has evolved over the last decade and its usefulness for measuring small displacements as occurs in engineering materials in tension and compression has been demonstrated by several investigators. For example, the method has been successfully applied to determine displacements and gradients of steel and aluminium with very high accuracy (McNeill et al. 1987) and has recently been applied to study tension, compression and bending behavior of small wood specimens and wood joints (Zink et al. 1995, Stelmokas et al. 1997). Durig et al. (1991) applied the method to determine stress intensity factors for aluminium in mixed-mode fracture and McNeill et al. (1987) used it to obtain mode I stress intensity factors for plexiglass. It has not been used to study fracture in wood.

The theory of digital image correlation has been described in detail by several researchers but a detailed treatment of the subject can be found in Sutton et al. (1983). The underlying principle of DIC and its application to obtain crack tip displacement fields in wood can be found in our earlier papers (Samarasinghe and Kulasiri 1998, 1999, 2000a, b).

4 Experimental Methods and Digital Image Correlation

Tensile specimens were prepared from three 5-m long and 140×20 mm^2 cross section kiln-dried boards of radiata pine obtained from a local sawmill. Specimen width, height, and thickness were 230, 140, and 20 mm, respectively, and a horizontal edge crack was cut parallel-to-grain (i.e. perpendicular to the height direction) as shown in Fig. 2a using a fine saw blade. The crack edge was sharpened to 20 mm length using a special knife prepared for the purpose to simulate a natural crack. The load application is in the height direction and crack propagates parallel-to-grain. A total of 35 specimens were prepared and the sample size was kept at this level due to the time consuming nature of image capture and processing. For each specimen, the absolute value of the

Fig. 2. Specimen configuration.

Fig. 3. Experimental set-up for tensile testing and image capture.

angle (θ) between crack plane and the RL plane was measured on the cross section. This was done by drawing, on the cross section, a line perpendicular to a growth ring that is cut by the crack (i.e. in the radial direction) as shown in Fig. 2a and measuring the angle between the crack and this line. The mean and the standard deviation of the angle was 12.3° and 9.5°, respectively. Another set of 12 bending specimens, of the size $300 \times 20 \times 20$ mm^3, corresponding to each fracture specimen were also prepared from an adjacent location on the board as shown in Fig. 2b to obtain a representative Young's modulus (E_L).

4.1 Tensile Testing and Image Capture

Tests were conducted on a computer controlled SINTECH material testing workstation. Special tensile jigs were manufactured to hold the specimen ends. The test set-up with equipment used to capture images is shown in Fig. 3. Specimens were speckled with black and white paint to obtain a random speckle pattern and were illuminated by a fiber optic ring light that allowed a very uniform level of illumination throughout the surface. Images (512×512 pixel) were captured by an Ikigami CCD (Charge Couple Device) video camera with 25 frames per second capture rate and a lens with ×20 magnification.

Prior to testing, a graph paper was placed against the specimen surface and its image was captured to calibrate the image distances to real distances. A typical resolution for the test set-up was 29 pixels/mm in the horizontal and 45 pixels/mm in the vertical directions, which represents a reasonably high resolution. Specimens were tested at a rate of 1 mm/min and for each specimen, 2 to 6 images were captured at various load levels up to failure. After failure, small pieces were cut from each specimen to measure moisture content and density based on oven-dry method. The mean and standard deviation for density were 393 kg/m^3 and 30.5 kg/m^3, respectively, and the same parameters for moisture content were 15.8% and 0.42%.
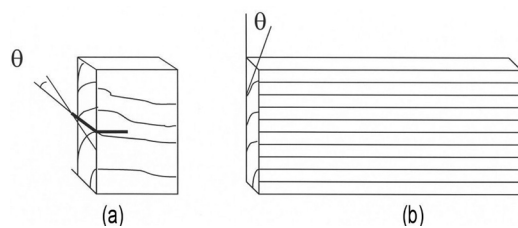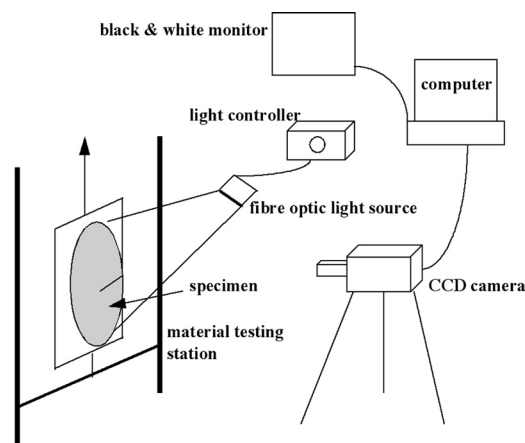
4.2 Bending Tests and Material Properties

Prior to testing the bending specimens for the determination of Young's modulus, the ring angle was measured for each specimen as the angle (θ) between the tangential sawn direction of the original board and a tangent to growth rings (Fig. 2b). Since 12 specimens were cut from each length position on the board, a broad range of θ values varying from 0° and 50° resulted. From geometric relations, this ring angle was equal to the angle between crack plane and RL plane measured on fracture specimens (Fig. 2). Each specimen was supported on two rollers with a span of 280 mm and a central vertical point load was applied parallel to the tangential direction of the original board. Tests were conducted on the SINTECH-MTS testing workstation at a rate of 1.5 mm/min. Displacement at the centre of the bottom surface was measured and Young's modulus calculated resulting in a mean and standard deviation of 5.88 MPa and 1.02MPa, respectively. The other required properties for the analysis were estimated from the Young's modulus as will be discussed later.

4.3 Crack Tip Displacement Analysis Using Image Correlation

The digital image correlation programme used in this study was Vic-2D (1998) and the accuracy of the program was ±0.02 pixels that amounts to ±0.00067 mm for images used in this study. An area of approximately 7 mm × 9 mm (200 × 400 pixels) in front of the crack was selected for analysis as shown in Fig. 4. The displacements of points located 0.5 mm apart horizontally, and 0.33 mm apart vertically were obtained. Thus from one pair of images corresponding to a load level, displacements of 370 to 420 points were determined. The programme provided vertical and horizontal displacements for each point.
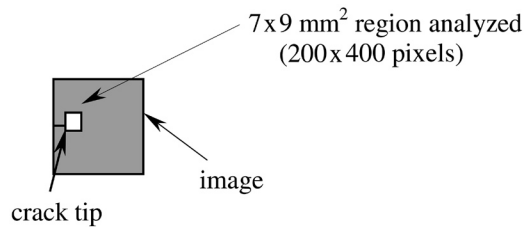

Fig. 4. Location of the analysed area of the image with respect to crack tip.

5 Computation of Stress Intensity Factors from Experimental Data

Stress intensity factors were determined by substituting experimental displacement field into theoretical field given by Eq. 1. This equation requires displacement perpendicular to the crack (v) and therefore, experimentally obtained vertical displacement was used in the analysis. According to fracture theory, crack tip is stationary and coincides with the origin of the co-ordinate system. The x-axis lies along the crack and y-axis is perpendicular to crack plane. The theoretical displacements are given with respect to the stationary crack tip. The data obtained from the digital image correlation underwent a major transformation to conform to this format. As stated earlier there were approximately 370 to 420 data points within a 7 mm × 9 mm area in front of the tip. Eq. 1 requires E_L, E_R, E_T, ν_{TL}, ν_{RL}, ν_{RT} and G_{LT} for the tip area through Eq. 2. For each fracture specimen, crack angle to RL plane was known and this angle was equal to the ring angle measured on the bending specimens. Therefore, out of the 12 corresponding bending specimens, the one with the ring angle closest to the crack angle to RL plane of the corresponding fracture specimen was selected and E_L for that specimen was used as the modulus representing the crack tip area. Other moduli were calculated in relation to E_L as in Bodig and Jayne (1982) according to the relation $E_L:E_R:E_T \approx 15:1.6:1$, and $E_L:G_{LT} \approx 15:1$. Poisson ratios were obtained from Table 3.1 of Bodig and Jayne (1982) as $\nu_{TL} = 0.033$, $\nu_{RL} = 0.041$, $\nu_{RT} = 0.47$.
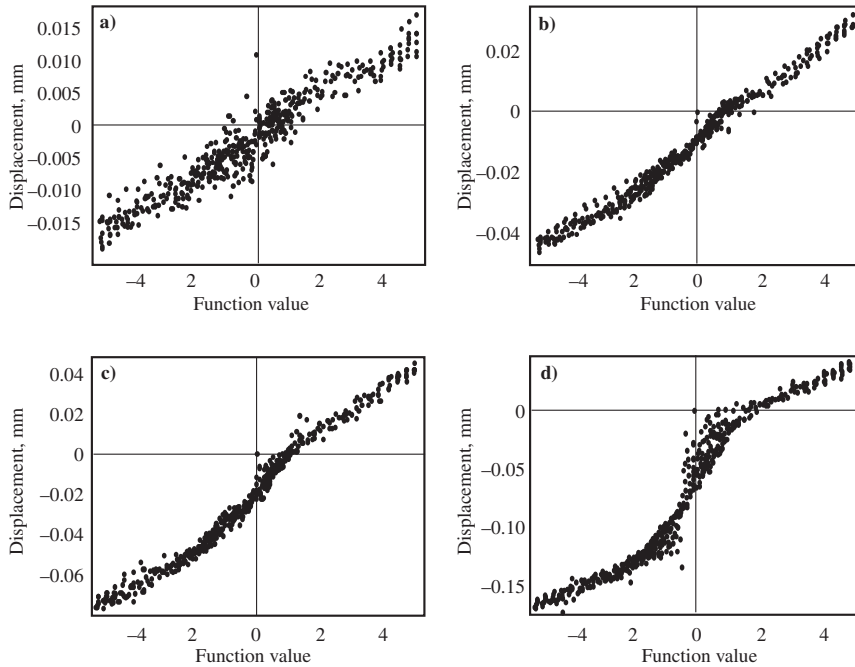
Fig. 5. Regression relationship between v displacement and function values (Eq. 1) for a typical specimen for the loads of a) 1 kN, b) 2 kN, c) 2.5 kN, and d) 3 kN.

The analysis was done on Mathematica (1997) as follows: For a particular load level, stress intensity factor was computed by equating the experimental tip displacement (v) of all the points in the direction of applied load to the theoretical displacement given in Eq. 1. For this purpose Eq. 1 was rearranged in the form shown below:

$$v = K_I \, f \, (r, \theta, E_i, G_{ij}, \nu_{ij}) \qquad (5)$$

and the experimental v displacement was regressed against the function, $f(r, \theta, E_i, G_{ij}, \nu_{ij})$ so that the slope of the regression line was the stress intensity factor, K_I. Basically, the right hand portion after K_I in Eq. 5 is the same as the right hand portion after K_I in Eq. 1. It is shown as a function of material properties, $f(r, \theta, E_i, G_{ij}, \nu_{ij})$, in Eq. 5 only for convenience. In the discussion below, it is called the function value. For a particular load, the function value for a point located a distance r and angle θ (Fig. 1) was obtained by inserting first material properties into Eq. 2 and by substituting its solutions, (μ_1, μ_2, q_1 and q_2), along with r and θ into Eq. 1. Refer to Sih et al. (1965) for detailed

form of these solutions. This way, the function values corresponding to all the points, (ranging from 370 to 420), for which experimentally measured displacements were available for that load level were obtained. Then, the experimentally determined v for each point was regressed against the corresponding function value as shown in any of the plots in Fig. 5 which will be explained later. The slope of the line according to Eqs. 1 and 5 is the stress intensity factor for that particular load. The procedure was then repeated for the other load levels and then for the other specimens. The analysis was successfully done on 27 specimens out of the 35 tested experimentally.

To demonstrate the results from the analysis, a review of the results for a single specimen is given here. For this specimen 4 load levels were analysed and they were 1 kN, 2 kN, 2.5 kN and 3 kN. The specimen failed at 3.1 kN. The load-displacement curve for this and all the other specimens were linear up to failure indicating the absence of any sub-critical crack growth. The experimental displacement and the function value regression plot for the four load levels is

shown in Fig. 5. The figure shows excellent linear plots for the first two load levels (Fig. 5a and 5b) and validates linear elastic fracture mechanics assumptions and indicates that a constant stress intensity factor uniquely determines the displacement at any point in the vicinity of the tip. Fig. 5c representing 2.5 kN is also mostly linear showing a slight nonlinear trend. Fig. 5d however, shows a nonlinear plot for the 3 kN load level indicating the breaking down of the linear theory, which may be due to large scale yielding caused by nonlinear behaviour at the tip. This issue is revisited later in the paper.

6 Comparison of Stress Intensity Factors Obtained from Crack-Tip Displacements and ASTM Standard Formula

Fig. 6a shows the experimental stress intensity factors for the four load levels along with the K_I computed from the ASTM standard formula (Eq. 3) for the specimen discussed in Section 5. For this and all other specimens, crack length to width ratio, a/w, was 0.143 for which the correction factor from the handbook formula (Eq. 4) was 1.25. Also t/w = 0.143 and a/t = 1.0, where t is thickness. The figure shows that the two stress intensity factors agree remarkably well for the two smaller load levels of 1 kN and 2 kN. The difference is slightly greater for the next 2.5 kN load and large for the 3 kN load just prior to failure at 3.1 kN load.

Out of the 27 specimens successfully analyzed, 11 (41%) exhibited a similar trend to that shown in Fig. 6a. Another 9 specimens (33%) showed a uniform gap between the two stress intensity factors up to the onset of non-linear trend on the experimentally tested specimen as shown in Fig. 6b for a typical specimen. The rest of the 7 specimens (26%) showed a widening gap from the start as in Fig. 6c shown for the worst specimen in this category. Thus, for 59% of specimens, the experimentally obtained stress intensity factor is larger than that obtained from the standard formula for
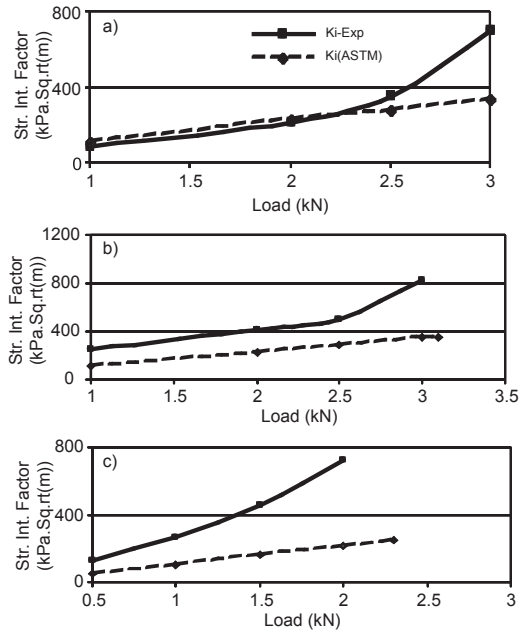

Fig. 6. Stress intensity factors based on crack-tip displacement and standard formula: a) an example of good agreement between the two, b) discrepancy with a uniform gap up-to the onset of nonlinearity and c) widening gap from the start.

all load levels. Furthermore, it is clearly seen that the crack-tip displacement based *critical* stress intensity factor K_{Ic} (fracture toughness) is always larger than that based on the ASTM formula.

Fig. 7 shows the stress intensity factor for all the specimens for the load levels at which images were captured and the corresponding ASTM standard values. This figure can be described as follows: for the 41% of the specimens mentioned earlier, the two values are in reasonably good agreement except closer to failure. The largest discrepancy is from the 26% of the specimens with a widening gap and the intermediate values are from the 33% of the specimens with a uniform gap.

6.1 Crack Tip Displacement Profiles to Explain Nonlinear Behaviour

One hypothesis to explain the discrepancy between the two stress intensity factors at higher load levels is the excessive deformations near

the tip. Some support for this hypothesis for the development of a plastic region near the tip comes from our previous paper (Samarasinghe and Kulasiri 2000a) where we presented displacement fields for wood (without a crack) in tension perpendicular-to-the grain. It demonstrated that displacement in this mode is uniform and analogous to that of rubber and we attributed the

uniform behaviour to lignin that deforms like an isotropic material. Therefore, it can be expected that, in the presence of a crack parallel-to-grain in tension (i.e. perpendicular grain loading), lignin carries and distributes much of the load and in the process can undergo large deformations near the highly stressed crack-tip region.

To examine the tip behaviour in detail, the experimentally measured vertical (v) displacement field at the tip was plotted as a function of distance (x,y), from the tip as shown in Fig. 8 for the same specimen and load levels (1 kN, 2 kN, 2.5 kN and 3 kN) depicted in Figs 5 and 6a. It can be seen from the figure that the v displacement increases with the load (Figs. 8a, b and c) and that a large increase is evident just prior to failure (Fig. 8d). These were the displacement fields used in the stress intensity factor analysis in this study. The first three produced a linear trend and the last represented a non-linear trend in Fig. 5 and 6a. Large displacements can indicate a growing plastic region. The reader may find a detailed analysis of displacement fields of wood in tension perpendicular-to-grain and crack tip
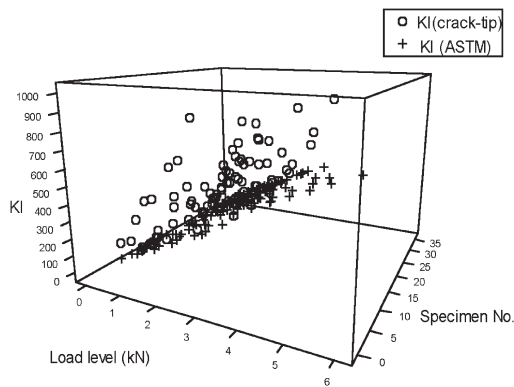

Fig. 7. Stress intensity factor for all specimens and all load levels based on crack-tip displacements and ASTM formula.
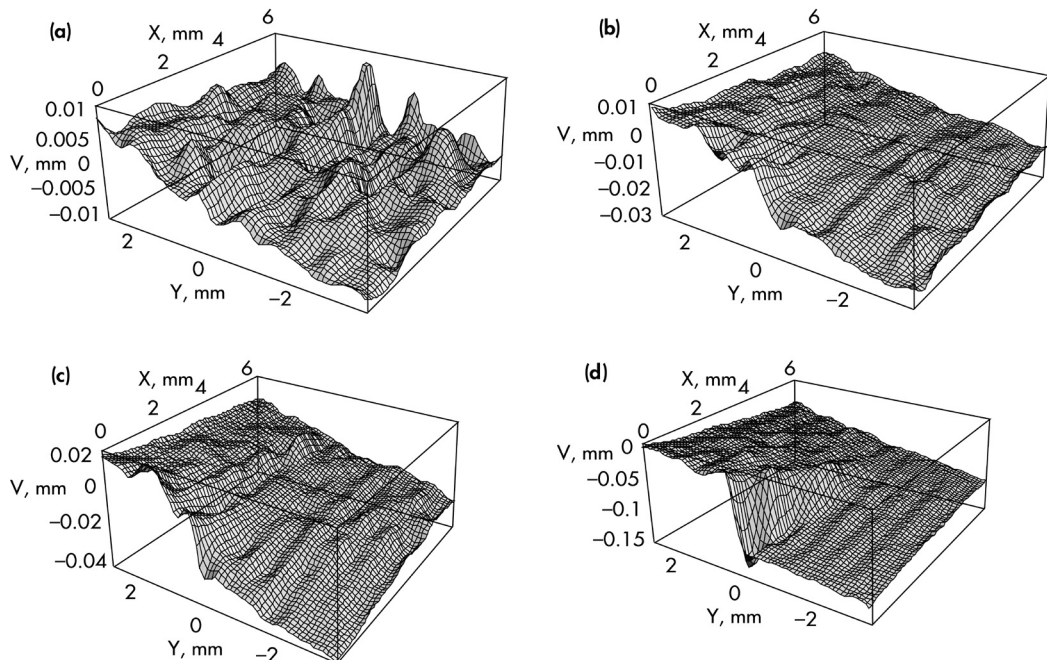

Fig. 8. Vertical displacement, v, fields for specimen depicted in Fig. 5 for the loads of a) 1 kN, b) 2 kN, c) 2.5 kN, and d) 3 kN.

displacements in our earlier papers (Samarasinghe and Kulasiri 2000a, b).

Another hypothesis to explain the discrepancy between the two stress intensity factors, especially at higher load levels, is that invisible microcracks develop near the tip area and these lead to the observed large displacements. The enlargement of the image near the crack tip region up to about 300% indicated some growth in the region for some specimens but no visible change at all for others that showed any nonlinear behaviour thus not providing any consistent visual clues for the observed phenomenon. These issues present interesting problems for further studies that will improve our understanding of the true material behaviour.

7 Critical Stress Intensity Factor (K_{Ic})

For most practical applications involving a crack, critical stress intensity factor (fracture toughness) is used in design. Fig. 9 shows the critical stress intensity factor K_{Ic} from the two approaches. The $K_{Ic(crack-tip)}$ is the fracture toughness obtained from the combined experimental and theoretical approach discussed earlier using images at the failure load. $K_{Ic(ASTM)}$ is the fracture toughness obtained from the ASTM standard formula for the same failure load. Since $K_{Ic(crack-tip)}$ is based on the local tip displacements, it does not require a geometry correction factor, which is an advantage of the proposed method. The ASTM formula, owing to its derivation, requires a geometry correction factor, F, which was obtained from Eq. 4. Clearly, the crack-tip based value is larger than that from the ASTM formula. The two were related nonlinearly through the following function with an R^2 value of 0.61.

$$K_{Ic}^{'} = 362 \ \ln(K_{Ic}) - 1369 \qquad (6)$$

where, K_{Ic}' and K_{Ic} denote $K_{Ic(crack-tip)}$ and $K_{Ic(ASTM)}$, respectively, and are abbreviated for equation clarity. With further validation, models such as these may be used to correct the standard values or obtain more accurate critical stress intensity factors.
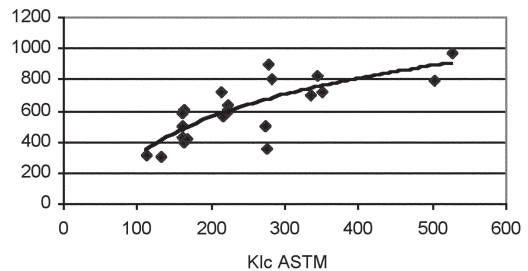

Fig. 9. The relationship between critical stress intensity factor from the crack-tip displacements and standard formula.

7.1 Influence of Angle between Original Crack Plane and RL Plane on K_{Ic}

Fig. 10 shows the original crack plane with respect to the final failure plane, which coincides with the RL plane. Fig. 11a shows the relationship between the K_{Ic} based on crack-tip displacements and the angle. It shows the trend that $K_{Ic(crack-tip)}$ increases with the angle. The two had a correlation coefficient (r) of 0.55. Fig. 11b shows the same relationship for the K_{Ic} from the ASTM formula and it also shows a similar trend. The correlation between the $K_{Ic(ASTM)}$ and the angle is 0.75. The results show that this angle is important and needs to be considered in the determination of critical stress intensity factor. The linear regression models developed to predict K_{Ic} from the angle alone resulted in an R^2 of 0.30 and 0.56 for crack-tip based and ASTM standard formula based values, respectively. Incorporation of measured density, moisture content and Young's modulus with the angle in a multiple linear regression did not produce a significant improvement. Clearly, there is a need to develop prediction models that incorporate physical variables and the angle described here from experiments designed for this purpose.
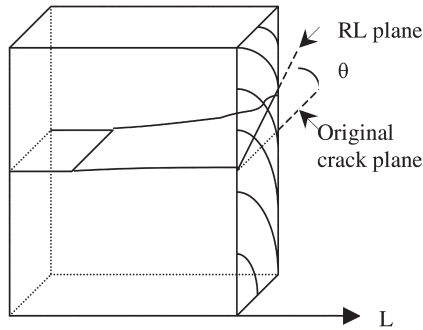
Fig. 10. Display of the original crack plane with respect to RL plane of eventual crack propagation for a typical specimen.
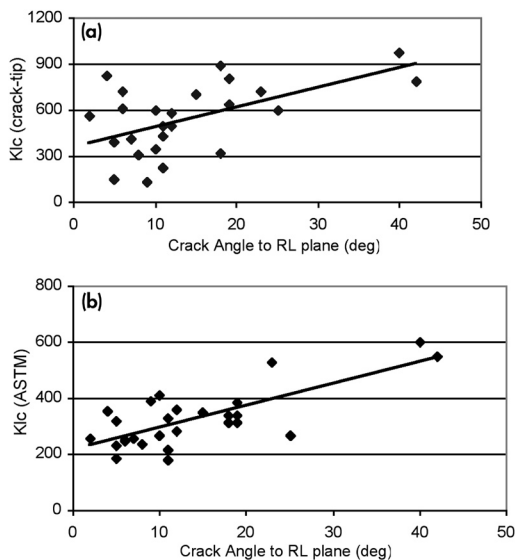

Fig. 11. Influence of crack angle to RL plane on the critical stress intensity factor derived from a) crack-tip displacements and b) ASTM standard formula.

8 Summary and Conclusions

In this study, crack-tip displacement fields obtained from digital image correlation were used in conjunction with orthotropic theory to obtain Mode-I stress intensity factors for wood in tension with an edge crack parallel-to-grain using representative material properties. The experimental data supported the fact that a constant stress intensity factor uniquely defines the crack tip displacements as suggested by the theory; however, this was not true for higher loads closer to failure. For 41% of the specimens, experimental stress intensity factor closely followed that obtained from the standard formula but deviated closer to failure. The crack-tip displacement fields showed a large increase in deflection at higher loads that we attributed to either large plastic deformations and/or micro-crack developments in the near-tip area. The other 59% of the specimens showed similar behaviour except that the crack-tip displacement based stress intensity factor was consistently larger than that based on the standard formula.

The critical stress intensity factor from the two approaches were nonlinearly related to each other and a logarithmic function with R^2 of 0.61 was fitted to express the relationship. With further validation through more studies, this type of formula can be used to correct the fracture toughness obtained from the standard formula, or the method proposed in this study can be used to obtain more accurate fracture toughness values that do not rely on geometry correction factors. This could eventually lead to improved strength predictions of timber. Results also found a strong positive correlation between the critical stress intensity factor and the angle between the original crack plane and the RL plane in which cracks propagate eventually.

This study is the first of its kind and the issues raised here need to be addressed through further study. Especially, conditions near the crack tip and ensuing plastic region and its size need to be investigated.

References

ASTM Standards-Metal testing. 1995. E 1290.

Bodig, J. & Jayne, B.A. 1982. Mechanics of wood and wood composites. Van Nostrand Reinhold Company, Inc.

Durig, B., Zhang, F., McNeill, S.R., Chao, Y.J. & Peter, III, W.H. 1991. A study of mixed mode fracture by photoelasticity and digital image analysis. Optics and Laser Engineering 14.

Gibson, L.J. & Ashby M.F. 1997. Cellular solids. 2nd Ed. Cambridge University Press, London.

Griffith, A.A. 1920. The phenomena of rupture and flow in solids. Philosophical Transactions, Series A 221: 163–198.

Irwin, G.R. 1957. Analysis of stresses and strains near the end of a crack traversing a plate. Journal of Applied Mechanics 24: 361–364.

— 1961. Plastic zone near a crack and fracture toughness. Sagamore Research Conference Proceedings 4. (as in Anderson, T.L. Fracture Mechanics – Fundamentals and Appl., 2nd Ed., 1994).

Mall, S., Murphy, J.F. & Shottafer, J.E. 1983. Criterion for mixed-mode fracture in wood. Journal of Engineering Mechanics 109: 681–690.

Mathematica (Version 3). 1997. Wolfram Research, USA.

McNeill, S.R., Peters, W.H. & Sutton, M.A. 1987. Estimation of stress intensity factor by digital image correlation. Engineering Fracture Mechanics 28(1): 101–112.

NeuroShell2. 1997. Ward Systems Group, Inc. USA.

Samarasinghe, S. & Kulasiri, G.D. 1998. Investigation of stress intensity factors of wood using image processing and orthotropic fracture theory. Proceeding of the 12th Engineering Mechanics Conference. p. 618–621.

— & Kulasiri, G.D. 1999. Fracture toughness of wood based on experimental near-tip displacements and orthotropic fracture theory. Proceedings of Pacific Timber Engineering Conference. p. 292–299.

— & Kulasiri, G.D. 2000a. Displacement fields of wood in tension based on image processing: Part 1. Tension parallel- and perpendicular-to-grain and comparisons with isotropic behavior. Silva Fennica 34(3): 251–259.

— & Kulasiri, G.D. 2000b. Displacement fields of wood in tension based on image processing: Part 2. Crack-tip displacements in Mode-I and Mixed Mode fracture. Silva Fennica 34(3): 260–273.

Sih, G.C., Paris, P.C. & Irwin, G.R. 1965. On cracks in rectilinearly anisotropic bodies. International Journal of Fracture Mechanics 1: 189–203.

Stelmokas, J.W., Zink, A.G. & Loferski, J.R. 1997. Image correlation analysis of multiple-bolted connections. Wood and Fiber Science 29(3): 210–227.

Sutton, M.A., Wolters, W.J., Peters, W.H., Rawson, W.F. & McNeill, S.R. 1983. Determination of displacements using an improved digital image correlation method. Image and Vision Computing 1(3): 133–139.

Tada, H., Paris, P.C. & Irwin, G.R. 1985. The stress analysis of cracks handbook. 2nd Ed., Paris Productions, Inc., St. Louis, USA.

Triboulot, P., Jodin, P. & Pluvinage, G. 1984. Validity of fracture mechanics concepts applied to wood by finite element calculation. Wood Science and Technology 18: 51–58.

Vic-2D. Version 2.1. 1998. Digital image correlation. Cimpiter, Inc. USA.

Westergaard, H.M. 1939. Bearing pressure and cracks. Journal of Applied Mechanics 6: 49.

Williams, M.L. 1957. On the stress distribution at the base of a stationary crack. Journal of Applied Mechanics 24: 109–114.

Zink, A.G., Davidson, R.W. & Hanna R.B. 1995. Strain measurement in wood using a digital image correlation technique. Wood and Fiber Science 27(4): 346–359.

Total of 24 references

Appendix 1. List of symbols.

v Vertical displacement of a point in the vicinity of crack (mm)

K_I Mode-I stress intensity factor (kPa$\sqrt{m}$)

K_{Ic} Fracture toughness ((kPa$\sqrt{m}$)

μ_1, μ_2, q_1 and q_2 Complex roots of the characteristic equation (Eq. 2)

σ Applied stress (MPa)

F Geometry correction factor

a Crack length (mm)

E_L Young's modulus in the longitudinal direction (MPa)

E_R Young's modulus in the radial direction (MPa)

E_T Young's modulus in the tangential direction (MPa)

ν_{RL} Poisson ratio in Radial-Longitudinal (RL) plane

ν_{RT} Poisson ratio in Radial-Tangential (RT) plane

ν_{TL} Poisson ratio in Tangential-Longitudinal (TL) plane

G_{LT} Shear modulus in Longitudinal-Tangential (LT) plane